

On quantum mechanical origin of higher-order Kerr effect in gases: Channel closure and resonances

P. Béjot^{1,*}, E. Cormier², E. Hertz¹, B. Lavorel¹, J. Kasparian³, J.-P. Wolf³, and O. Faucher¹

¹ *Laboratoire Interdisciplinaire CARNOT de Bourgogne,*

UMR 6303 CNRS-Université de Bourgogne, BP 47870, 21078 Dijon, France

² *Centre Lasers Intenses et Applications, Université de Bordeaux-CNRS-CEA,*
UMR 5107, 351 Cours de la Libération F-33405 Talence, France and

³ *Université de Genève, GAP-Biophotonics, Chemin de Pinchat 22, 1211 Geneva 4, Switzerland*

We perform full 3D time-dependent Schrödinger equation (TDSE) in atomic hydrogen under strong-field excitation. Our calculation reveals a supplementary, quasi-instantaneous negative term as compared to the weak-field model of polarizability widely used to evaluate the non-linear refractive index. This term is closely related to ionization channel closure, providing an interpretation to the similar inversion intensities observed experimentally in various gases. It stems from the interaction of the electrons promoted into the continuum with their parent atom, which imposes to consider an effective electron mass during the pulse duration.

PACS numbers: 34.80.Dp, 42.65.An

Atoms and molecules exposed to a nonresonant intense (10-100 TW/cm²) laser field exhibit highly nonlinear dynamics that has motivated a wealth of experimental and theoretical studies and led to the observation of phenomena such as above-threshold ionization (ATI) [1] or high-harmonics generation (HHG) [2], whose interest has been boosted by the discovery of attosecond pulses [3]. Understanding these processes requires describing atomic and molecular dynamics under strong-field excitation, in which the electric field is so intense that transitions can be enhanced by dynamic resonances, leaving the atom in a coherent superposition of excited states. Because of this complex dynamics, the atomic optical response cannot be described as a perturbative series of the field. Instead, the atom dynamics and its associated polarization must be evaluated at each time during the interaction by solving the time-dependent Schrödinger equation (TDSE) describing the interacting atom.

Most of the attention focused on the strong-field response of the system at harmonic frequencies, as opposed to the fundamental one. The imaginary and real parts of the susceptibility at the fundamental frequency relate to absorption and dephasing of the driving electric field, respectively. The nonlinear part of the latter, known as the all-optical Kerr effect, induces an intensity-dependent refractive index described through the nonlinear refractive index n_2 . It plays a major role in the nonlinear propagation of ultrashort and ultra-intense laser pulse, and in particular in the filamentation of ultrashort laser pulses [4–7].

Filamentation has attracted a great interest due to its spectacular potential applications [8–13]. It is generally described as a dynamic balance between Kerr self-focusing and defocusing by the free electrons originating from ionization during the interaction. Since the typical

intensity in filaments (50 TW/cm² [14, 15]) is of the same order as that observed in HHG or ATI, it seems natural to wonder whether the Kerr effect, a third order non-linear process, would already deviate from a pure cubic variation law in this regime.

Saturation and even inversion of the Kerr effect was indeed reported between 19 and 33 TW/cm² in major air components [16, 17], and empirically described as negative higher-order Kerr effect (HOKE).

A similar inversion intensity was obtained in a quantum description of hydrogen, and predominantly attributed to continuum-continuum transitions [18–20]. Similar results have been recently reported in atomic silver [21] and in H₂⁺ [22], as well as with TDSE calculations in a one-dimensional Dirac potential [23], and by considering Kramers-Kronig relations and multiphoton ionization rates [24]. However, a laser-induced transient grating was also proposed as an alternative interpretation of the measured Kerr inversion [25].

In this Letter, we show that 3D non-perturbative ab-initio calculation of the interaction between the strong laser field and an hydrogen atom offer a detailed quantum mechanical description of the Kerr saturation and inversion. The usual model of polarizability, describing a purely third-order Kerr medium together with a negative plasma contribution, misses a substantial negative contribution above the ionization channel closure ($I_0 \geq 32$ TW/cm² in atomic hydrogen). This contribution is due to the over-acceleration of the electrons during the excitation pulse because they interact with their parent atom, and results in the quasi-instantaneous inversion of the Kerr effect. It can be described as an electron with an effective mass moving in the field and identified to the empirically-introduced HOKE [16, 17]. It is further influenced by field-induced resonances that leave several excited states significantly populated at the end of the pulse.

Finally, considering the need for a computationally-efficient modeling of the high-field-atom interaction for

* pierre.bejot@u-bourgogne.fr

inclusion in e.g. filamentation models, we propose a practical parametrization of the non-linear refractive index based on the results of the full TDSE calculations.

Within the dipole approximation, the TDSE describing the electron wavefunction $|\psi\rangle$ evolution in the presence of an electric field $\mathbf{E}(t)$ linearly polarized along the axis z can be written as:

$$i\frac{d|\psi\rangle}{dt} = (H_0 + H_{\text{int}})|\psi\rangle, \quad (1)$$

where $H_0 = \nabla^2/2 - 1/r$ is the hydrogen atom Hamiltonian, $H_{\text{int}} = -\mathbf{E}(t) \cdot \mathbf{r}$ (resp. $H_{\text{int}} = \mathbf{A}(t) \cdot \boldsymbol{\pi}$, where $\mathbf{A}(t)$ is the vector potential such that $\mathbf{E}(t) = -\partial\mathbf{A}/\partial t$ and $\boldsymbol{\pi} = -i\nabla$) is the interaction term expressed in the length gauge (resp. velocity gauge). The time-dependent wavefunction $|\psi\rangle$ is expanded on a finite basis of B-splines allowing much faster computation than with eigenfunctions of the Hamiltonian H_0 [26]:

$$\psi(\mathbf{r}, t) = \sum_{l=0}^{l_{\text{max}}} \sum_{i=1}^{n_{\text{max}}} c_i^l(t) \frac{B_i^k(r)}{r} Y_l^0(\theta, \phi), \quad (2)$$

where B_i^k and Y_l^m are B-spline functions and spherical harmonics, respectively. The basis parameters (l_{max} , n_{max} , k and the spatial box size) and the propagation parameters are chosen to ensure the convergence. Unless specified, calculations are performed in the velocity gauge ensuring fast convergence. The atom is initially in the ground state (1s) and the electric field E is expressed as $E(t) = E_0 \cos(t/\sigma_t)^2 \cos(\omega_0 t)$, where ω_0 is the central pulsation of the laser, $\sigma_t = 2N/\omega_0$, and N the total number of optical cycles in the temporal window. The simulations are performed for a laser wavelength of 800 nm and pulse durations (FWHM of intensity) of 23 fs, 29 fs, 47 fs, 58 fs, and 93 fs (corresponding to $N=24$, 30, 48, 60 and 96 cycles respectively).

The microscopic polarization $p(t)$ and the medium polarizability α at the driving frequency ω_0 are defined in atomic units as:

$$p(t) = \langle \psi(t) | r \cos \theta | \psi(t) \rangle \quad (3)$$

$$\alpha(\omega_0) = \frac{p(\omega_0)}{E(\omega_0)}, \quad (4)$$

where $p(\omega)$ (resp., $E(\omega)$) is the Fourier transform of $p(t)$ (resp., $E(t)$). The macroscopic polarization P is then calculated as $P(t) = \mathcal{N}p(t)$, with \mathcal{N} the atom density per volume unit. Its nonlinear part P_{NL} and the nonlinear polarizability $\Delta\alpha$ are calculated as:

$$P_{\text{NL}}(t) = P(t) - \mathcal{N} \lim_{I_0 \rightarrow 0} \alpha(I_0)E(t), \quad (5)$$

$$\Delta\alpha(I_0) = \alpha(I_0) - \lim_{I_0 \rightarrow 0} \alpha(I_0), \quad (6)$$

where I_0 is the peak intensity of the pulse. As shown in Fig. 1, this instantaneous non-linear polarization envelope follows the intensity profile in the low-field regime

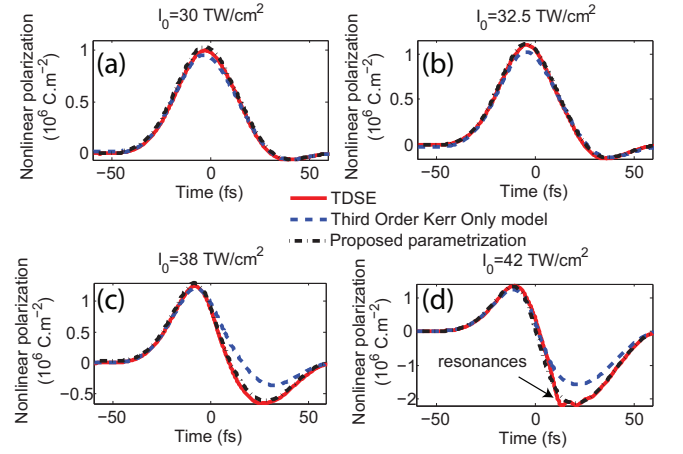


Figure 1. (Color online) Nonlinear polarization envelope as a function of time for a 30 (a), 32.5 (b), 38 (c), and 42 (d) TW/cm^2 48 cycles pulse.

($I_0 < 30 \text{ TW}/\text{cm}^2$), as expected for a purely cubic Kerr effect. However, above $\sim 32 \text{ TW}/\text{cm}^2$, a transient, time-retarded negative contribution develops on the second half of the pulse. This contribution is significantly underestimated by the commonly used third-order Kerr only (TOKO) model of polarizability (blue dashed line in Fig. 1), which treats the Kerr effect as a purely cubic and the electrons ejected during the interaction as free particles accelerated by the field:

$$P_{\text{NL, TOKO model}}(t) = \epsilon_0 \left(n_2 I(t) - \frac{\mathcal{N} \rho_{\text{PPT}}(t)}{\rho_c} \right) E(t), \quad (7)$$

where ρ_{PPT} is the ionization probability calculated with the PPT theory [28], $\rho_c = m_e \omega_0^2 \epsilon_0 / q^2$ is the critical plasma density, n_2 is the nonlinear index of the medium, ϵ_0 is the vacuum permittivity, and m_e and q are the electron mass and charge, respectively.

The non-linear polarizability of the atom at the fundamental frequency ω_0 increases linearly with the pulse peak intensity, and then saturates and reverses its sign (Fig. 2). This peak intensity is in line with previous works [18–20, 22, 23] and similar for all investigated pulse durations. It also corresponds to the development of the discrepancy between the polarizabilities calculated by TDSE and by the TOKO model. This extra negative term scales with the fourth power of the incident peak intensity, consistent with its empirical identification as a $\chi^{(9)}$ term, i.e. a negative $n_8 I_0^4$ contribution to the refractive index [16]. The physical origin of this negative term can be inferred by observing that Eq. (7) deviates from the full TDSE model as soon as the intensity exceeds the 10-photon channel closure ($I_0 \geq 32 \text{ TW}/\text{cm}^2$, see Figure 2), and further increases above the 11-photon ionization channel closure at $57 \text{ TW}/\text{cm}^2$. The channel closure therefore appears to constitute a key ingredient of the negative non-linear transient contribution to the polar-

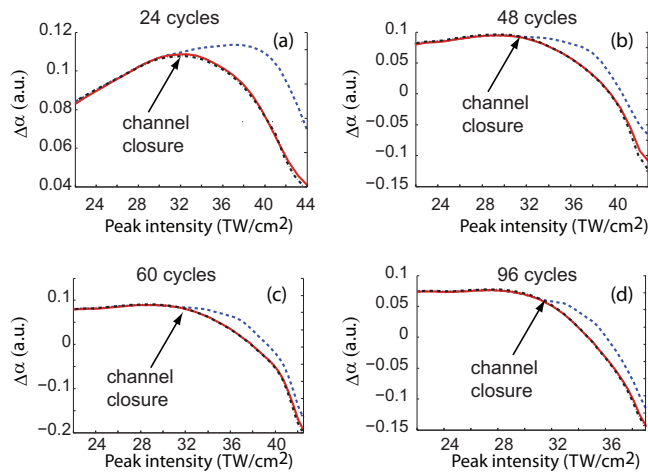


Figure 2. (Color online) Nonlinear polarizability as a function of peak intensity for 24 (a), 48 (b), 60 (c) and 96 (d) cycles pulse calculated with TDSE (red solid line), TOKO model (blue dashed line) and proposed parametrization (black dotted-dashed line), respectively.

izability. Its impact appears similar to the one induced by the ionization suppression mechanism [27] but will take place at lower intensities. The major constituents of the air, as well as most usual gases, exhibit ionization channel closures in the same intensity range as hydrogen (21.5 and 48 TW/cm² in Ar, 18.5 and 32 TW/cm² in O₂, and 25 and 51 TW/cm² in N₂). This may explain the comparable inversion intensities found in Ar, N₂ and O₂ [16].

Beyond the channel closure, excited states dynamically shift with intensity. The resulting dynamical resonances induce efficient post-pulse population of excited states. In particular, 2d, 3d, and 1-4g states are resonantly populated after the interaction with pulses of 40 TW/cm² peak intensity, impacting the atomic polarizability (Fig. 1(d)) and the associated nonlinear refractive index. This time-dependent effect becomes even more pronounced for longer pulses (>50 fs). It may therefore seem natural to investigate which transitions (e.g., to bound-bound, bound-continuum, and continuum-continuum transitions as defined in [18]) contribute more to the Kerr saturation and inversion.

However, specific states or state groups, like bound or continuum states, are unphysical (because gauge-dependent) during the interaction. As a consequence, continuum states cannot be considered as constituting a plasma, which limits the relevance of identifying states or transitions during the interaction. The gauge-dependence of the partial polarizations, illustrated in Fig. 3(a,b), prevents any rigorous interpretation in terms of the partial polarizations, i.e., any identification of specific transitions (or, alternatively, of the "plasma") as responsible for the Kerr saturation and inversion [18–21]. The fact that the partial polarizability α_{CC} related to

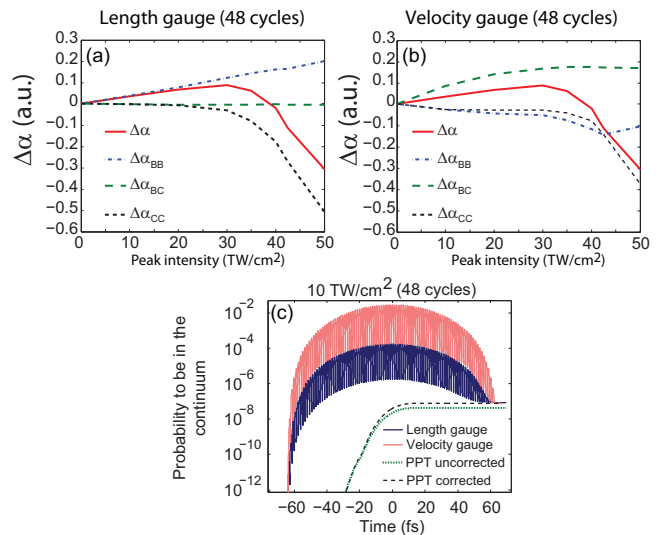


Figure 3. (Color online) Nonlinear polarizability as a function of intensity calculated in (a) the length and (b) velocity gauge respectively. $\Delta\alpha_{BB}$, $\Delta\alpha_{BC}$, and $\Delta\alpha_{CC}$ refer to the partial non-linear polarizabilities related to bound-bound, bound-continuum and continuum-continuum transitions, respectively. (c) Probability of the electron to be in the continuum during a 48 cycles 10 TW/cm² pulse calculated in the length and velocity gauges respectively, compared with the output of the PPT formula.

continuum-continuum transitions provides the main negative contribution to the total polarizability in both the velocity and the length gauges does not contradict this statement, since it does not imply any similar behavior in other gauges.

As illustrated in Fig. 3(c), the probability to find the electron in the continuum, $\rho = 1 - \langle \psi_B(t) | \psi_B(t) \rangle$, being the bound part of the electron wavefunction, is gauge-dependent within several orders of magnitude during the pulse. Consequently, during the pulse, a plasma density cannot be defined. Rather, all electrons interact with their parent atom, which as discussed below can be modelled by introducing an effective mass $m_{e,eff}$ affecting the electron acceleration. Conversely, at the end of the pulse, both E and A are zero so that the electron density becomes physical. Simultaneously, the electrons leave their parent atom and the post-pulse system can indeed be described as a plasma.

Owing to the complexity of the TDSE calculations, practical purposes requiring repeated computation of the non-linear refractive index, like the simulation of laser filamentation, require a simple (i.e., computationally efficient) parametrization of the non-linear refractive index. The minimal complexification of Equation (7) allowing to fit the TDSE results expresses as:

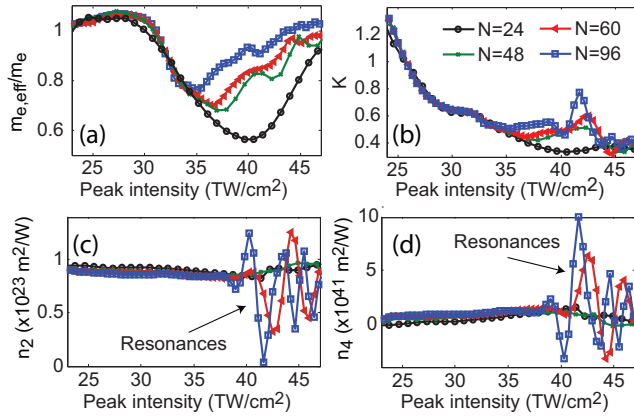


Figure 4. (Color online) Electron effective mass $m_{e,\text{eff}}$ (a), normalization factor K of the PPT ionization probability (b), n_2 (c), and n_4 (d) as a function of peak intensity for $N=24$ (black dots line), $N=48$ (green crosses line), $N=60$ (red triangles line), and $N=96$ (blue circle line).

$$P_{\text{NL,corr}}(t) = \epsilon_0 \left(n_2 I(t) + n_4 I^2(t) - \frac{K(I_0) \mathcal{N} \rho_{\text{PPT}}(t)}{\rho_{c,\text{eff}}(I_0)} \right) E(t). \quad (8)$$

where $n_4 I(t)^2$ is an instantaneous fifth-order term, K a normalization factor imposed to the PPT theory so as to accurately reproduce the post-pulse ionization probability (See Fig. 3(c)), and $\rho_{c,\text{eff}} = m_{e,\text{eff}}(I_0) \omega_0^2 \epsilon_0 / q^2$ is the critical plasma density corrected, during the pulse, for the effective electron mass $m_{e,\text{eff}}$ introduced above. The latter term corresponds to the quasi-instantaneous intra-pulse defocusing contribution accounting for most of the discrepancy between the HOKE calculations and the TOKO model (Figs. 1 and 2).

Figure 4 displays the parameters n_2 , n_4 , K and $m_{e,\text{eff}}$ as fitted to match the results of the TDSE calculations. The ratio $m_{e,\text{eff}}/m_e$ keeps close to unity before the channel closure ($I \approx 32 \text{ TW/cm}^2$), and subsequently decreases down to almost 0.5 (Fig. 4a). The resulting fit is excellent over the full range of pulse durations and peak powers investigated in the present work (Figs. 1 and 2). It may therefore be expected to improve the quantitative match between filamentation models and experiments

It should be noted that the continuum electrons over-accelerate only during the pulse. After the interaction, ejected electrons are far away from their parent ion and therefore behave as free particles, so that their effective mass relaxes to m_e at the end of the pulse. This negative effect is therefore much similar (except for the slight delay, compatible with the experimental temporal reso-

lution), to the HOKE introduced empirically to describe the experimental observations of Kerr saturation and inversion [16, 17].

Finally, as shown in Fig. 5, the non-linear polarizability saturates and reverses only at frequencies within the bandwidth of the incident pulse spectrum. As a conse-

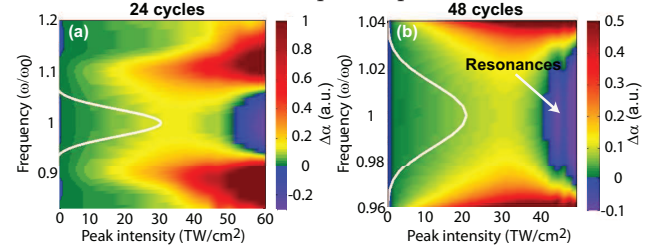


Figure 5. (Color online) Spectral dependence of the non-linear polarizability for (a) 24 and (b) 48 cycles.

quence, a weak probe beam of a different wavelength will not be sensitive to the polarizability inversion. This unexpected finding offers a clear explanation to the apparent contradiction between measurements performed at a single wavelength, which exhibit Kerr saturation and inversion [16, 17, 29], and two-color experiments, that do not [29–31].

As a conclusion, TDSE calculations show that the non-linear polarizability of hydrogen saturates and reverses its sign around 30 TW/cm^2 , an intensity at which refractive index inversion (aka HOKE) is observed [16, 17]. In this high-field regime, characterized by ionization channel closure, the electrons promoted into the continuum do not significantly interact with their parent ion and cannot be treated as free charged particles during the pulse. Rather, an effective electron mass must be considered, which affects the intra-pulse effective critical plasma density. The resulting quasi-instantaneous supplementary defocusing term can be identified as the HOKE [16, 17], and illustrates that media ionizing under strong-field illumination cannot be treated as a plasma. Since channel closure occurs at a similar intensity in all usual gases, our findings explain the similar HOKE inversion intensities in all major air constituents. Our work therefore sheds a new light on the Kerr effect in the strong-field regime typical of, e.g., laser filamentation.

Acknowledgments. This work was supported by the Conseil Régional de Bourgogne, the *FASTQUAST* ITN Program of the 7th FP. JPW acknowledges financial support from the ERC advanced grant "FilAtmo". EC and PB thank O. Peyrusse and the CRI-CCUB for CPU loan on their respective multiprocessor servers.

[1] J.H. Eberly, J. Javanainen, and K. Rzazewski, Phys. Rep. **204** (5), 331-383 (1991)

[2] M. Ferray *et al.*, J. Phys. B **21**, L31 (1988)

[3] P. Antoine, A. L'Huillier, and M. Lewenstein, Phys. Rev.

- Lett. **77** (7), 1234-1237 (1996)
- [4] S. L. Chin *et al.*, Can. J. Phys. **83**, 863 (2005).
- [5] L. Bergé *et al.*, Rep. Prog. Phys. **70**, 1633 (2007).
- [6] A. Couairon and A. Mysyrowicz, Phys. Rep. **441** 47 (2007).
- [7] J. Kasparian and J.-P. Wolf, Opt. Express **16**, 466 (2008).
- [8] J. Kasparian *et al.*, Science **301**, 61-64, (2003).
- [9] J. Kasparian *et al.*, Opt. Express. **16**, 5757 (2008)
- [10] P. Rohwetter *et al.*, Nature Photon. **4**, 451 (2010)
- [11] S. Tzortzakis *et al.*, Opt. Lett. **27**, 1944 (2002)
- [12] C.P. Hauri *et al.*, Appl. Phys. B **79**(6), 673-677 (2004)
- [13] D.S. Steingrube *et al.*, New J. Phys. **13**, 043022 (2011)
- [14] J. Kasparian, R. Sauerbrey, S. L. Chin Applied Physics B **71**, 877 (2000)
- [15] A. Becker *et al.* Applied Physics B **73**, 287 (2001)
- [16] V. Loriot *et al.*, Opt. Express **16**, 13429 (2009); Erratum in Opt. Express **18** 3011 (2010)
- [17] V. Loriot *et al.*, Laser Physics **21** (7), 1319-1328 (2011)
- [18] M. Nurhuda, A. Suda, and K. Midorikawa, Phys. Rev. A **66**, 041802 (2002)
- [19] M. Nurhuda, A. Suda, and K. Midorikawa, New J. Phys. **10**, 053006 (2008)
- [20] P. Kano, M. Brio, and J.V. Moloney, Comm. Math. Sci. **4** (1), 53-80 (2006)
- [21] E.A. Volkova, A.M. Popov, and O.V. Tikhonova, JETP Lett. **94** (7), 519-524 (2011)
- [22] E. Lorina *et al.*, Physica D **241**(12), 1059-1071 (2012)
- [23] A. Teleki, E.M. Wright, and M. Kolesik, Phys. Rev. A **82**, 065801 (2010)
- [24] C. Brée, A. Demircan, and G. Steinmeyer, Phys. Rev. Lett. **106**, 183902 (2011)
- [25] J.K. Wahlstrand and H.M. Milchberg, opt. Lett. **36**(19), 3822-3824 (2011)
- [26] H. Bachau *et al.*, Rep. Prog. Phys. **64**, 1815-1942 (2001)
- [27] F. Morales *et al.* PNAS **108**, 16906 (2011)
- [28] A. M. Perelomov, V. S. Popov, and M. V. Terentev, JETP, **23**(6), 924 (1966)
- [29] R.J. Levis, Private communication
- [30] J. K. Wahlstrand *et al.*, Phys. Rev. Lett., **107**, 103901 (2011)
- [31] J. M. Brown *et al.*, Opt. Lett. **37**, 1064 (2012)